European Journal of Radiology 121 (2019) 108734

Contents lists available at ScienceDirect

European Journal of Radiology

journal homepage: www.elsevier.com/locate/ejrad

Research article

Quantitative dynamic contrast-enhanced MR imaging for the preliminary prediction of the response to gemcitabine-based chemotherapy in advanced pancreatic ductal carcinoma

Wei Tang[a,1], Wei Liu[a,1], Hai-Ming Li[a], Qi-Feng Wang[b], Cai-Xia Fu[c], Xiao-Hong Wang[a], Liang-Ping Zhou[a,*], Wei -Jun Peng[a,*]

[a] Department of Radiology, Fudan University Shanghai Cancer Center, Department of Oncology, Shanghai Medical College, Fudan University, 270 Dongan Road, Xuhui District, Shanghai, 200032, China
[b] Department of Pathology, Fudan University Shanghai Cancer Center, Department of Oncology, Shanghai Medical College, Fudan University, 270 Dongan Road, Xuhui District, Shanghai, 200032, China
[c] MR Applications Development, Siemens Shenzhen Magnetic Resonance Ltd., Shenzhen, China

ARTICLE INFO

Keywords:
Pancreatic ductal carcinoma
Tumor response
Gemcitabine
Dynamic contrast-enhanced MR

ABSTRACT

Purpose: To investigate the role of the quantitative parameters of dynamic contrast-enhanced MR imaging (DCE-MRI) in the prediction of the response to chemotherapy in pancreatic ductal carcinoma (PDC).
Method: Forty patients with histologically confirmed PDC who underwent quantitative DCE-MRI were retrospectively analyzed. All patients were divided into groups of responders and nonresponders. DCE-MRI parameters, including the volume transfer constant (K^{trans}), the extracellular extravascular volume fraction (v_e), the rate constant (k_{ep}) and the initial area under the concentration curve in 60 s (iAUC60), were measured and compared. DCE-MRI parameters were obtained from different ROIs.
Results: The values of K^{trans} in responders with peripheral, whole tumor slice, and adjacent non-tumorous region ROIs were significantly higher than those in nonresponders ($P = 0.015$, 0.043, and 0.025, respectively). Responders showed a significantly higher k_{ep} with peripheral area ROI compared with nonresponders ($P = 0.013$). Ve and iAUC60 with all ROIs were not significantly different between responders and nonresponders ($P = 0.140$-0.968). Kep with periphery ROI showed the highest area under the ROC curve (AUC) of 0.806, but there were no statistical differences when compared with values of K^{trans}.There were statistically significant differences for DCE-MRI parameters among four ROIs (all $P < 0.05$). All parameters showed good to excellent intra and interobserver agreement.
Conclusions: Quantitative parameters derived from DCE-MRI might be a potential predictor of response to gemcitabine in patients with PDC. Perfusion parameters were diverse depending on the location of the ROI on different tumoral and peritumoral areas.

1. Introduction

The prognosis of pancreatic ductal carcinoma (PDC) is poor, with a 5-year survival rate of less than 7 percent [1], especially in advanced PDC. In the last two decades, the gemcitabine-based chemotherapy regimen had been the mainstay of first-line therapy for advanced PDC [2]. However, gemcitabine resistance in some patients can develop within weeks of chemotherapy initiation. Finding a reliable and non-invasive way for predicting the gemcitabine resistance as early as possible is significant for individual treatment and better prognosis.

Abbreviations: AIF, Artery input function; AUC, Area under the curve; CA, Celiac axis; DCE-MRI, Dynamic contrast-enhanced magnetic resonance imaging; DWI, Diffusion-weighted imaging; FOV, Field of view; GRE, Gradient echo; iAUC60, Initial area under the concentration curve in 60s; ICC, Intraclass correlation coefficients; k_{ep}, Rate constant; K^{trans}, Volume transfer constant; MVD, Micro-vessel density; NSCLC, Non-small cell lung cancer; PD, Progressive disease; PDC, Pancreatic ductal carcinoma; PR, Partial response; SV, Splenic vein; ROI, Region of interest; SD, Stable disease; SMA, Superior mesenteric artery; SMV, Superior mesenteric vein; SS-EPI, Single-shot echo planar imaging; ST, Slice thickness; TE, Time of echo; TR, Time of repetition; v_e, Extracellular extravascular volume fraction; VEGF, Vascular endothelial growth factor; VIBE, Volume-interpolated breath-hold examination

* Corresponding authors.
E-mail addresses: zhoulp2006@163.com (L.-P. Zhou), weijun6002@163.com (W.-J. Peng).
[1] These authors contributed equally to this work.

https://doi.org/10.1016/j.ejrad.2019.108734
Received 9 April 2019; Received in revised form 15 August 2019; Accepted 27 October 2019

Dynamic contrast-enhanced magnetic resonance imaging (DCE-MRI), as a tool of functional MRI, has been widely mentioned in oncology in recent years. The quantitative and semiquantitative parameters of DCE-MRI could provide the information of vascular permeability and blood perfusion features of tissues *in vivo*. For PDC, DCE-MRI has played important roles in differential diagnosis [3], assessment of anti-angiogenic therapy [4], and assessment of resectability of pancreatic tumors [5]. Moreover, quantitative parameters of DCE-MRI can reflect some features of the tumor microenvironment [6], which may be related to drug resistance and poor prognosis. Therefore, we performed this study to define the potential correlations between quantitative parameters originating from DCE-MRI and the incidence of gemcitabine resistance.

2. Materials and methods

2.1. Patients

We analyzed a total of 78 patients with suspected PDC experiencing DCE-MRI scanning before treatment in our institute from October 8, 2016 to September 30, 2018. These patients all experienced biopsy guided by ultrasound endoscopy. We further excluded 38 patients (Fig. 1): the pancreatic lesions were not PDC confirmed by biopsy (n = 2); the reexamination time was not as scheduled (n = 14); the therapeutic regimen was changed in the follow-up period (n = 7); the DCE-MRI images showed obvious breathing artifacts (n = 8); the patient was lost to follow-up (n = 7). Ultimately, 40 patients with unresectable lesions were recruited in our study. According to the 2017 NCCN guideline [7,8], unresectable diseases indicated both locally advanced lesions and/or distant metastases. For PDC, locally advanced diseases indicated tumours invading (> 180° involvement) the superior mesenteric artery (SMA), or celiac axis (CA), or first jejunal arterial branches or had aortic involvement. Unresectable venous involvement included unreconstructible superior mesenteric vein (SMV) or splenic vein (SV) involvement, or contact with the most proximal jejunal branches that drained into the SMV. Any distant metastases placed the patient in the unresectable category. The clinical features were listed in Table1. These patients experienced the same chemotherapy regimen—gemcitabine combined with abraxane. Every chemotherapeutic cycle last four weeks, including three-week chemotherapy and one-week interval. Every patient experienced at least 6 cycles. The evaluations of curative effects were performed after every two courses of treatment on the basis of RECIST 1.1 criteria [9]. According to the evaluation results and referring to the study of Zhang Z [10], 40 patients were grouped into responders (PR-PR-PR, SD-PR-PR or SD-SD-PR) and nonresponders (SD-SD-SD, SD-SD-PD, PR-PD-PD, PD-PD-PD) (Table1). When a patient was grouped into nonresponders, other palliative therapy regimen would be considered. This study was approved by the institutional review board.

2.2. DCE-MRI examination protocols

The equipment used for DCE-MRI examinations was a 3 T MR scanner (MAGNETOM Skyra, Siemens Healthcare, Erlangen, Germany). An integrated body coil was used for excitation, and the signal was received using a dedicated 18-channel body coil in combination with a 32-channel integrated spine coil. The MR images included T2-weighted imaging with BLADE sequences, fat-suppressed T1-weighted imaging with 3D GRE volumetric interpolated breath-hold examination (VIBE), diffusion-weighted imaging (DWI) with single-shot echo planar imaging (SS-EPI). T1 maps obtained by conventional VIBE sequences with flip angles of 3° and 15°, and DCE scanning with free-breathing golden-

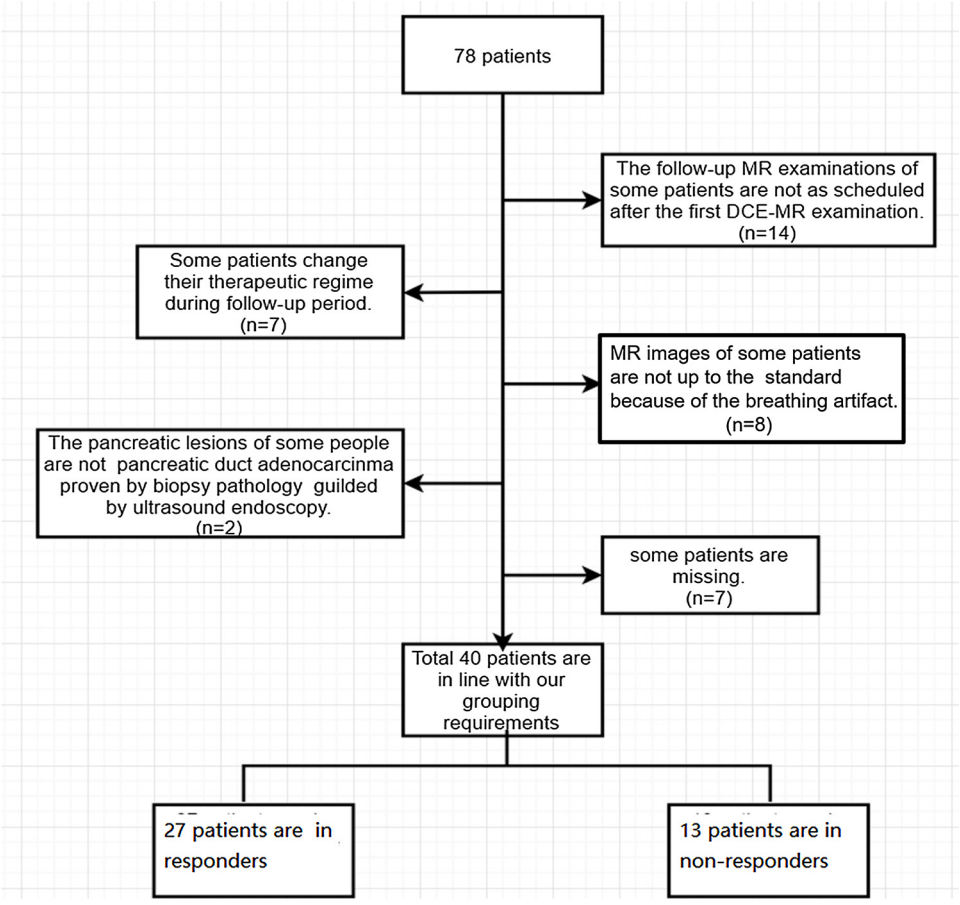

Fig. 1. Flow chart for screening out enrolled patients.

Table 1
Clinical characteristics and groups.

Variables		values
Age(year)[a]		61.8 ± 7.9(41–76)
Gender		
	Male	19(47.5 %)
	Female	21(52.5 %)
Location		
	Head and neck	15(37.5 %)
	Body and tail	25(62.5 %)
Ca19.9(U/ml)		
	0–37	5(2.5 %)
	> 1000	11(27.5 %)
	≤1000	24(60 %)
Size(cm)		4.92 ± 1.36(2–8.5)
Hepatic metastases		
	Yes	13(32.5 %)
	No	27(67.5)
lymph node metastases	Yes	25(62.5 %)
	No	15(37.5 %)
Stage[b]		
	IIB	3(7.5 %)
	III	20(50 %)
	IV	17(42.5 %)
Groups	Three follow-up results[c]	NO. Responders (n = 27, 67.5 %) Non-responders (n = 13, 32.5 %)
	PR-PR-PR	8
	SD-PR-PR	7
	SD-SD-PR	12
	SD-SD-SD	8
	SD-SD-PD	3
	PR-PD-PD	1
	PD-PD-PD	1

PR, partial response; SD, stable disease; PD, progressive disease.
[a] means ± standard deviation.
[b] The stages are based on the 8th American Joint Committee on Cancer staging.
[c] Follow-up results are based on RECIST 1.1.

angle radial VIBE sequence, which was previously proven to be feasible for performing DCE-MRI analysis [11,12]. The scanning parameters are as follows. T2WI: time of repetition (TR), 3500 ms; time of echo (TE), 83 ms; flip angle, 91°; imaging matrix, 256*256; slice thickness (ST), 4 mm; interval, 0.8 mm; field of view (FOV), 380 mm*380 mm. Fat-suppressed T1WI: TR, 120 ms; TE, 1.4 ms; flip angle, 70°; imaging matrix, 320*320; ST, 3.5 mm; interval, 0.7 mm; FOV, 380 mm*380 mm. DWI : TR, 6100 ms; TE, 59 ms; imaging matrix, 98*120; ST, 5 mm; interval, 0 mm; FOV, 380 mm*310 mm; b values: 50, 800 and 1000s/mm^2. T1-mapping: TR, 5.01 ms; TE, 2.3 ms; flip angle, 3° and 15°; imaging matrix, 64; ST, 8 mm; interval, 1.6 mm; FOV, 380 mm*380 mm. Free-breathing DCE: TR, 3.78 ms; TE, 1.72 ms; flip angle, 12°; imaging matrix, 256; ST, 3 mm; interval, 0.6 mm; FOV, 380 mm*380 mm. The image acquisition time of every DCE sampling time was 2.8 s, and every DCE sampling was 52 frames. We totally acquired 34 phases in one whole tumor DCE sequences and the duration was 4 min and 27 s. All patients were asked to breathe quietly during the examination and to place their hands above their heads. The 15 mL of contrast agent (Gd-DTPA, Magnevist, Bayer Healthcare) was injected with an intravenous bolus at a rate of 1.5 mL/s, followed by a 10 mL saline flush at 2 mL/s after 10 s from the beginning of the DCE sequence. The scanning ranged from the liver to the upper poles of the kidneys.

2.3. MR imaging data interpretations

We exported images from the MR scanner and imported them into a computer with a DCE-MRI Toolbox (prototype software; Siemens Healthcare, Erlangen, Germany), which was programmed for calculating DCE-MRI parameters. We conducted the following procedure stepwise: loading imaging data in the software, correcting the motion of dynamic series and T1 maps, selecting the arterial input function (AIF), choosing the pharmacokinetic model, performing the calculation, and reading the parameters based on different regions of interest (ROIs). The AIF we used was measured by the time-concentration curve of a length of abdominal aorta at branching off the celiac trunk in axial plane by a semi-automatic filling tool (Fig. 2A, B). The DCE-MRI evaluations were based on the Tofts model.

ROIs were manually drawn by two radiologists(radiologist 1 and 2, with 5 and 7 years of experience in abdominal imaging diagnosis, respectively) on pancreatic DCE-MRI images. To better delineate the tumor, they also interpreted other sequences such as DWI and T1 fat-suppressed images. Inter-observer agreement was evaluated from radiologist 1 and 2. To evaluate the intra-observer agreement of all parameters, the radiologist 1 redrew the ROIs two months after the first drawing on the DCE-MRI images of all patients, and blinded to the previous measurement. According to the studies of Wu L [13] and Kim J H [14], the placements of the ROIs were around the periphery with a rim of thicknesses from 3 to 5 mm (Fig. 2E), and in the core part with diameters of 6–10 mm at the largest tumor slice (Fig. 2F). Additionally, we also delineated a large ROI on the axial images at the largest slice, including the whole tumor slice (Fig. 2G), and an arc ROI along the edge of the tumor with 3- to 5-mm thickness at upstream nontumorous pancreas parenchyma (Fig. 2H). For best showing the tissue perfusion situation, all ROI placements were drawn manually to bypass peripheral fat, artifacts, necrosis, cystic necrosis/cystic components, and blood vessels in the tumor and pancreatic ducts according to T1WI, T2WI and T1WI-based DCE-MRI images. All ROIs were drawn in the arterial phase for the maximum contrast of tumor and normal pancreatic tissue. Finally, we calculated a selection of parameters, including the volume transfer constant(K^{trans}), the rate constant(k_{ep}), the extracellular extravascular volume fraction(v_e) and the initial area under the concentration curve in 60 s (iAUC60).

2.4. Statistical analysis

Statistical tests were performed in SPSS20.0 (Chicago, IL) and MedCalc15.2.2 (Mariakerke, Belgium), and the statistical diagrams were delineated in GraphPad Prism 5 (GraphPad Software, San Diego, CA, USA). First, logistic regression of clinical variables was performed to indicate if clinical features played a role in response to chemotherapy. Second, we computed the intra- and interobserver intraclass correlation coefficients (ICC). Third, if parameters met the normality and homogeneity of variance, an independent sample *t*-test was performed to screen out those parameters that could distinguish responders and nonresponders, or the Mann-Whitney *U* test was conducted. We then performed multivariable receiver operating characteristic curve (ROC) analysis to compare the values of these statistically significative parameters in predicting the curative effect of gemcitabine-based chemotherapy. Finally, we referred the study of Kim J H [14] and Wu L [13], and then performed a paired *t*-test to investigate the differences in quantitative parameters of DCE-MRI among peripheral, core, and whole tumor slice and adjacent nontumorous regions. Statistical analyses were considered to indicate a significant difference when *P* values were less than 0.05.

3. Results

3.1. The impacts of some clinical variables in response to chemotherapy

The *P* values of these clinical variables (gender, age, location, size, hepatic metastasis, lymph node metastases and Ca19.9) were from 0.144 to 0.986, and all larger than 0.05 (Table2).

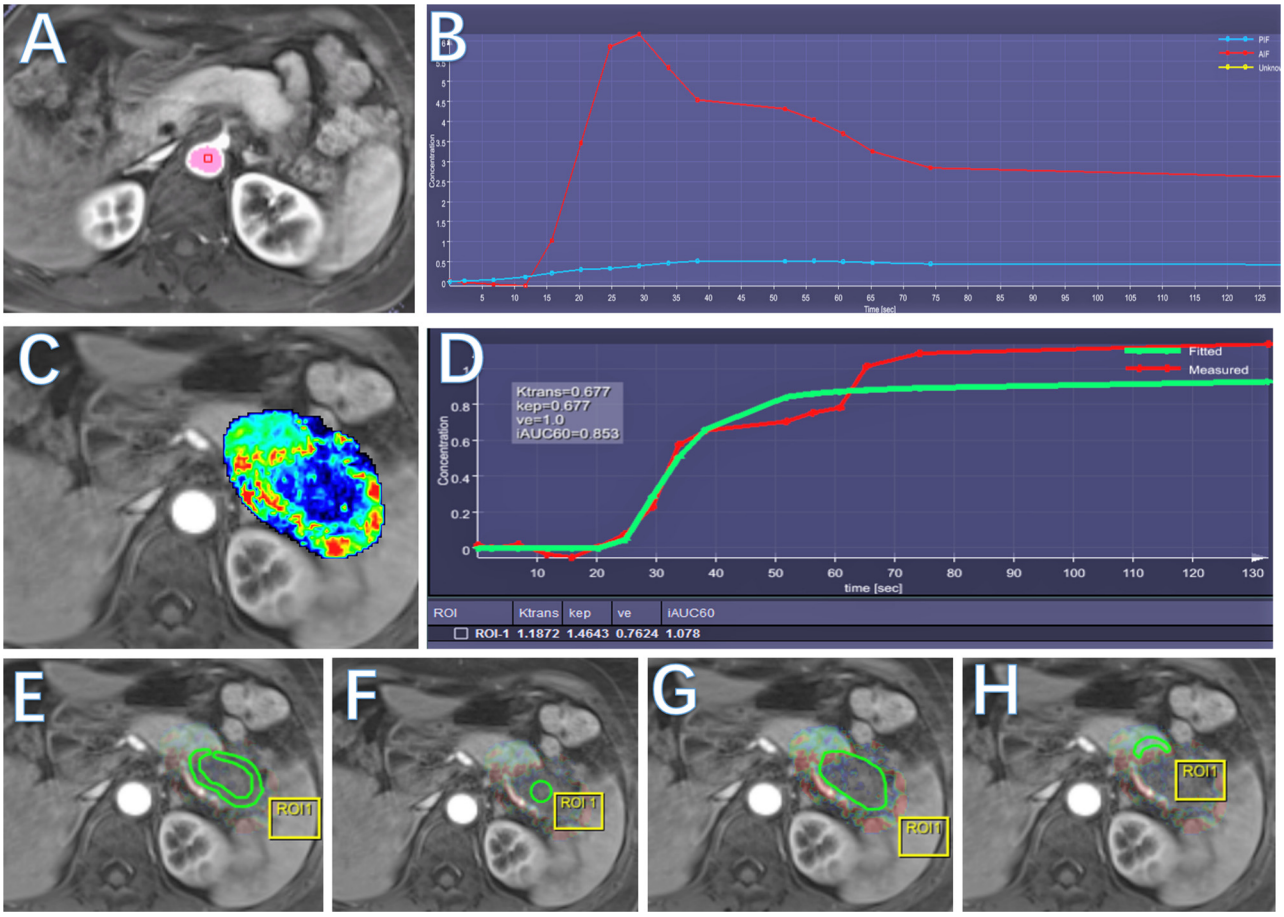

Fig. 2. Delineation of different ROIs.
A, the region used to compute the artery input function (AIF); B, the AIF curve; C Pixel-by-pixel color map for K^{trans} obtained with region-of-interest analysis. Calculated values of each pixel in the ROI can be seen with red, yellow, and blue being the high, middle, and low values, respectively. D, the time to concentration of contrast agent and the quantitative parameters of DCE-MRI in ROI. E-H: the ROI placements in the tumorous periphery, core region, whole slice and the adjacent nontumorous region.

Table 2
Logistic regression of clinical variable between responders and nonresponders.

Variable	B	S.E,	Sig.	Exp (B)	95% CI of Exp (B)	
					lower bound	upper bound
gender	−0.147	0.904	0.871	0.863	0.147	5.073
age	0.015	0.050	0.771	1.015	0.920	1.119
location	−0.343	0.938	0.715	0.710	0.113	4.463
size	−0.196	0.302	0.516	0.822	0.454	1.486
Hepatic metastases	−1.454	0.994	0.144	0.234	0.033	1.641
lymph node metastases	−1.612	0.880	0.487	0.542	0.097	3.041
Ca 19.9	−0.922	0.659	0.162	2.513	0.691	9.139
constant	−0.081	4.676	0.986	1.085		

B: partial regression coefficient, S.E: standard error, Sig.: P value, Exp(B): odds ratio.

3.2. Differences in quantitative parameters of DCE-MRI between responders and nonresponders

These parameters had good reproducibility and stability, with interobserver ICCs from 0.544 to 0.815 and intra-observer ICCs from 0.612 to 0.843 (Table3). These parameters were significantly different between responders and nonresponders: K^{trans} (1.813 ± 0.829 vs. 1.175 ± 0.516) in peripheral areas, k_{ep} (1.835 ± 0.684 vs. 1.302 ± 0.393) in peripheral areas, K^{trans} (1.556 ± 0.770 vs. 1.073 ± 0.431) in whole tumor slices and K^{trans} (2.242 ± 1.007 vs. 1.641 ± 0.606) in adjacent nontumorous areas. K^{trans} values of responders in the tumorous periphery, whole tumor slices and adjacent

Table 3
Stable and reproducible analyses of these quantitative parameters of DCE-MRI.

ROIs	quantitative parameters			
	K^{trans}	k_{ep}	v_e	iAUC60
ICCs in intra observer				
periphery	0.843 (0.723–0.913)	0.774 (0.610–0.874)	0.612 (0.365–0.776)	0.750 (0.576–0.860)
core	0.840 (0.717–0.912)	0.837 (0.714–0.91)	0.597 (0.352–0.765)	0.721 (0.533–0.842)
whole slice	0.815 (0.596–0.894)	0.833 (0.676–0.913)	0.693 (0.488–0.825)	0.707 (0.498–0.836)
adjacency	0.821 (0.687–0.902)	0.828 (0.698–0.905)	0.752 (0.577–0.861)	0.714 (0.520–0.838)
ICCs between inter observers				
periphery	0.792 (0.369–0.915)	0.711 (0.477–0.843)	0.688 (0.484–0.821)	0.702 (0.418–0.847)
core	0.815 (0.679–0.898)	0.777 (0.615–0.875)	0.676 (0.464–0.815)	0.747 (0.572–0.858)
whole slice	0.744 (0.566–0.856)	0.764 (0.597–0.868)	0.544 (0.250–0.739)	0.731 (0.545–0.848)
adjacency	0.766 (0.599–0.870)	0.741 (0.560–0.854)	0.631 (0.398–0.787)	0.702 (0.516–0.883)

ICCs, intraclass correlation coefficients.

Table 4
Comparison of parameters derived from DCE-MRI between responders and nonresponders.

variables	responders	non-responders	*P* value
periphery			
$K^{trans}(min^{-1})$	1.813 ± 0.829	1.175 ± 0.516	0.015*
$k_{ep}(min^{-1})$	1.835 ± 0.684	1.302 ± 0.393	0.013*
v_e	0.789 ± 0.177	0.704 ± 0.149	0.140
iAUC60(mmol/s)	1.215 ± 0.407	1.049 ± 0.275	0.193
core			
$K^{trans}(min^{-1})$	1.318 ± 0.837	0.912 ± 0.404	0.107
$k_{ep}(min^{-1})$	1.481 ± 1.231	0.714 ± 0.677	0.289
v_e	0.714 ± 0.228	0.677 ± 0.185	0.619
iAUC60(mmol/s)	0.952 ± 0.327	0.956 ± 0.345	0.968
whole slice			
$K^{trans}(min^{-1})$	1.556 ± 0.770	1.073 ± 0.431	0.043*
$k_{ep}(min^{-1})$	1.656 ± 0.727	1.289 ± 0.345	0.094
v_e	0.778 ± 0.176	0.702 ± 0.140	0.182
iAUC60(mmol/s)	1.110 ± 0.324	1.013 ± 0.292	0.369
adjacency			
$K^{trans}(min^{-1})$	2.242 ± 1.007	1.641 ± 0.606	0.025*
$k_{ep}(min^{-1})$	1.855 ± 1.000	1.641 ± 0.606	0.271
v_e	0.615 ± 0.235	0.501 ± 0.226	0.154
iAUC60(mmol/s)	1.005 ± 0.348	0.946 ± 0.336	0.614

* P value less than 0.05 indicates statistical significance.

nontumorous regions were higher than those of nonresponders. The k_{ep} value of responders in the tumorous periphery was higher than that of nonresponders, but the differences were not evident in ROIs of the whole tumor slice and adjacent nontumorous regions. In addition, the differences of v_e and iAUC60 values in these ROIs between responders and nonresponders were not statistically significant. With respect to all parameters in core ROIs between responders and nonresponders, none of the differences were statistically significant. The specific data are shown in Table4.

3.3. Multivariable ROC analysis of significantly different variables between responders and nonresponders

The AUCs of k_{ep} and K^{trans} of the tumorous periphery and of K^{trans} of whole tumor slice and adjacent nontumorous regions were 0.806, 0.744, 0.735 and 0.681, respectively. Their sensitivities were 77 %, 62 %, 85 %, and 85 %, and their specificities were 85 %, 85 %, 59 % and 56 %, respectively (Table5). The differences of the AUCs were not statistically significant, and the *P* values ranged from 0.1797 to 0.7706, which were all more than 0.05 (Fig. 3).

3.4. Differences of the DCE-MRI parameters in different placement ROIs

All of the DCE-MRI parameters in the peripheral region (K^{trans}, k_{ep}, v_e, iAUC60: 1.605 ± 0.795, 1.662 ± 0.651, 0.761 ± 0.171, 1.162 ± 0.374) were apparently higher than those of the core region (K^{trans}, k_{ep}, v_e, iAUC60: 1.186 ± 0.745, 1.399 ± 0.691, 0.702 ± 0.213, 0.953 ± 0.328). Compared with the respective parameters of the adjacent nontumorous area (K^{trans}, k_{ep}, v_e, iAUC60: 2.047 ± 0.933, 1.738 ± 0.951, 0.578 ± 0.235, 0.986 ± 0.341), the K^{trans} values in periphery, core of tumor and whole tumor slice were all

Table 5
Multivariable ROC analyses of statistically significant parameters of DCE-MRI between responders and nonresponders.

variable	cutoff	sensitivity (%)	specificity (%)	AUC	95% CI
$k_{ep\ peri}$	1.318	77	85	0.806	0.651–0.914
K^{trans}_{adjac}	2.022	85	56	0.681	0.515–0.819
K^{trans}_{peri}	1.149	62	85	0.744	0.581–0.868
K^{trans}_{whole}	1.300	85	59	0.735	0.572–0.862

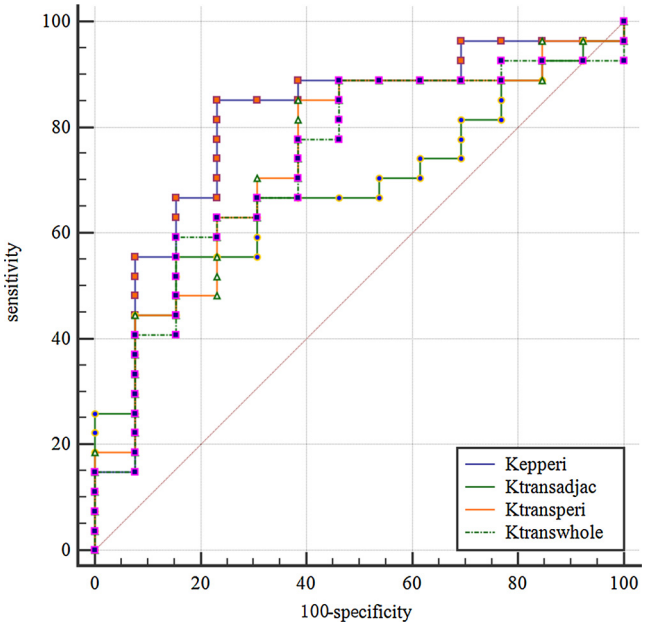

Fig. 3. Multi-variable ROC analyses of the statistically significant parameters.

lower, the v_e values in these regions were all larger, and the k_{ep} values in these regions did not show a significant difference. With regards to iAUC60, only the value in the peripheral region of tumor was slightly larger, while the values in the core and the whole tumor slice had no statistically difference. The data were shown in Fig. 4.

4. Discussion

A recent study had shown that quantitative parameters of DCE-MRI might be potential predictors of treatment responses [15]. The study performed by Zhang Z et al. [10] indicated that K^{trans}, particular that of the peripheral tumor region, could predict the early response to radiotherapy in advanced uterine cervical carcinoma. For advanced esophageal cancer [16], nasopharyngeal carcinoma [17], and locally advanced non-small cell lung cancer (NSCLC) [18], perfusion parameters were also valuable in predicting and assessing therapeutic response. In our study, some quantitative perfusion parameters in responders to gemcitabine combined with abraxane were obviously different from those in nonresponders, indicating that DCE-MRI might be useful in making decisions about treatment regimens for advanced PDC.

In our study, these clinical variables (gender, age, location, size, hepatic metastasis, lymph node metastases and Ca19.9) had no impacts on grouping based on RECIST1.1. The K^{trans} of PDC lesions were obviously higher in responders than in nonresponders, which was similar to the findings in some previous studies. Bali M A. et al. [19] found that K^{trans} was negatively related to fibrosis. For PDC, abundant extracellular matrix (ECM) was present around cancer cells and enfolded a bank of fibroblasts and myofibroblasts, which was in correlation with gemcitabine resistance [20,21]. The robust fibroinflammatory response generated inordinately high interstitial fluid pressures, induced vascular collapse, and then presented substantial barriers to drugs [22]. Moreover, gemcitabine was a cytotoxic drug that could promote cancer cell apoptosis, and its therapeutic effects depended on its concentration around cancer cells [21]. Consequently, a higher K^{trans} value in PDC represented lower fibrosis, bringing a relatively better response to drugs. However, in the study performed by Liu K. et al. [6], the negative correlation between K^{trans} and fibrosis was not significant. Therefore, further investigations are needed. Additionally, the study of Liu K [6] also showed that K^{trans} was positively related with the expression of tumor vascular endothelial growth factor (VEGF), a key regulator of

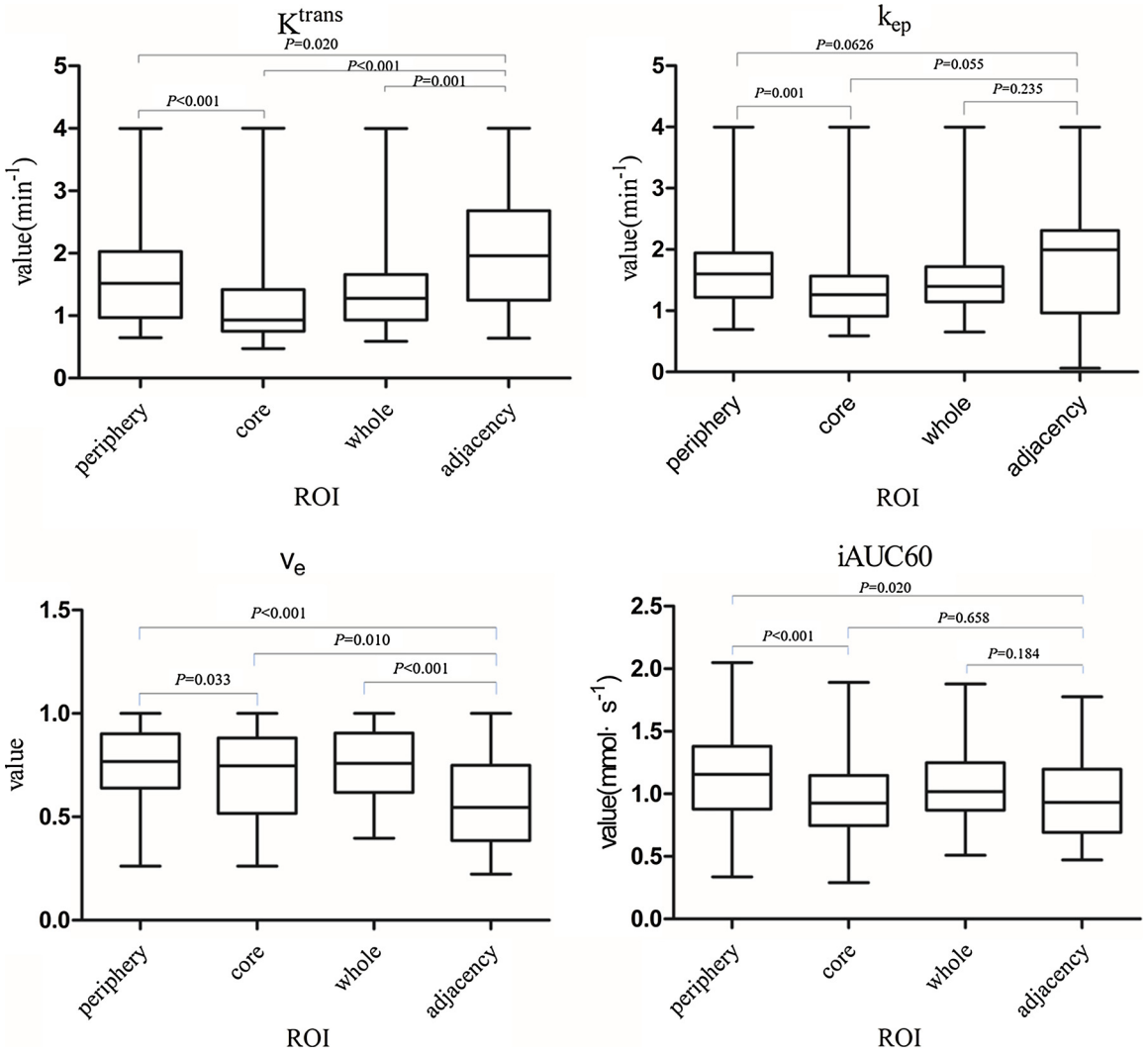

Fig. 4. Comparisons of different quantitative parameters of DCE-MRI in different ROIs.
Box-and-whisker plot of DCE parameters in different ROIs. Boxes = interquartile range, whiskers = range of all values, horizontal line within box = median. The unit of K^{trans} is min^{-1}. The unit of k_{ep} is min^{-1}. Ve is unitless. The unit of iAUC60 is mmol·s^{-1}. The statistical difference has significant, When *P* value is less than 0.05.

tumor angiogenesis, and its increase correlated with poor prognosis of PDC [23,24]. Therefore, the predictive value of K^{trans} could also be elucidated from this perspective.

Interestingly, the k_{ep} of the peripheral region of PDC tumors in responders was also higher than in nonresponders, which could also be explained by the negative correlation between k_{ep} and fibrosis [6]. A higher k_{ep} corresponded to a better delivery of therapeutic drugs into the interstitial space, leading to a better response. Moreover, k_{ep} was negatively correlated with Ki-67, which was positively associated with cell proliferation [25]. Hence, a higher k_{ep} value would show a relatively lower rate of cancer cell proliferation.

Apart from the value of quantitative parameters of PDC lesions, we also found that the K^{trans} of adjacent nontumorous regions in responders was higher than that in nonresponders. We provided a hypothesis that a higher K^{trans} value in a adjacent nontumorous region indicated the relatively lower degree of tumor invasiveness. The reasons may be as follows: i) the K^{trans} of PDC was influenced predominantly by blood flow, because the features of abnormal leakiness, fragility, and structural instability of PDC tumor vasculature were not significant due to the collapse caused by abundant stroma in the microenvironment [19]; ii) some tumor compartments were implanted in the adjacent nontumorous areas due to the invasive growth of malignant tumors; iii) the blood perfusion of PDC was apparently less than that of normal pancreatic parenchyma. The weaker the invasiveness in adjacent nontumorous region was, the greater the blood flow might be. Therefore, the K^{trans} would be higher.

We also found k_{ep} value in tumourous periphery showed the highest AUC of 0.806, compared with other parameters (K^{trans} in tumorous periphery, whole tumor slice and adjacent nontumorous regions), but there were no statistically significant differences.

Some studies had focused on the correlation of v_e and iAUC60 with the tumor microenvironment. Ve showed a significantly positive correlation with tumor fibrosis [6] and collagen content [19]. IAUC60 showed the positive correlation with micro-vessel density (MVD) and percentage of vascular endothelial growth factor (VEGF) positive cells [13]. As mentioned above, tumor fibrosis, MVD and VEGF were associated with prognosis of PDC. In our study, however, both v_e and iAUC60 had no significant difference between responders and nonresponders.

In addition, K^{trans} values in tumors were all lower than in the adjacent nontumorous region, which was consistent with the study performed by Kim, J H et al. [14]. However, v_e in tumors and iAUC60 in tumorous periphery was higher, and k_{ep} between tumors and adjacent nontumorous region had no statistical difference, which were not consistent with the previous study [14]. This might be due to the bias of small sample size. The quantitative parameters of DCE-MRI were all

higher in the tumorous periphery than in the tumorous core, which was similar to the findings in the study performed by Wu, L. et al. [13]. The heterogeneity of PDC, caused by fibrosis, glandular formation and mucin production, might be the reason of the difference of DCE parameters in different regions [26,27]. It was easy to understand that tumor activity, including angiogenesis, proliferation and other effects, were vigorous in the periphery while weak in the core.

There were some limitations in our study. First, the sample size was small, because CT scanning replaced DCE-MRI for some patients. Second, the follow-up period was relatively short (ranging from 24 to 32 weeks) after the beginning of initial chemotherapy, and further follow-up data should be collected. Third, the ROIs were drawn manually, although we tried our best to keep the ROIs consistent, some bias were unavoidable. Finally, our present study did not investigate the correlation between quantitative DCE-MRI and histopathological markers (VEGF, MVD, tumor cell density and tumor fibrosis). Further study is needed to support our results.

In conclusion, K^{trans} and k_{ep} computed by DCE-MRI might be potential predictors of response to gemcitabine in PDC patients. The values of some quantitative parameters of DCE-MRI were influenced by the placements of ROIs.

Funding

This study has received funding by Shanghai Health and Family Planning Commission Youth Fund Project (20174Y0242) and Special Fund of Radiology of Fudan University Shanghai Cancer Center (YX201702).

Guarantor

The scientific guarantor of this publication is Dr. Wei-Jun Peng.

Statistics and biometry

One of the authors (Wei Liu) has significant statistical expertise.

Informed consent

Written informed consent was obtained from all subjects (patients) in this study.

Ethical approval

Institutional Review Board approval was obtained.

Study subjects or cohorts overlap

No study subjects or cohorts has been previously reported.

Methodology

- retrospective analysis
- diagnostic, prognostic and observational study
- performed at one institution

Declaration of Competing Interest

The authors of this manuscript declare no relationships with any companies, whose products or services may be related to the subject matter of the article.

Acknowledgements

The authors would like to thank Lei Yue, Xiao-Xing Hu, and Hai-Ming Li for their technical support throughout the preparation of this manuscript.

References

[1] R.L. Siegel, K.D. Miller, A. Jemal, Cancer Statistics, 2017, CA Cancer J. Clin. 67 (1) (2017) 7–30, https://doi.org/10.3322/caac.21387.
[2] H.R. Burris, M.J. Moore, J. Andersen, M.R. Green, M.L. Rothenberg, M.R. Modiano, et al., Improvements in survival and clinical benefit with gemcitabine as first-line therapy for patients with advanced pancreas cancer: a randomized trial, J. Clin. Oncol. 15 (6) (1997) 2403–2413, https://doi.org/10.1200/JCO.1997.15.6.2403.
[3] K. Liu, P. Xie, W. Peng, Z. Zhou, Assessment of dynamic contrast-enhanced magnetic resonance imaging in the differentiation of pancreatic ductal adenocarcinoma from other pancreatic solid lesions, J. Comput. Assist. Tomogr. 38 (5) (2014) 681–686, https://doi.org/10.1097/RCT.0000000000000120.
[4] M.F. Akisik, K. Sandrasegaran, G. Bu, C. Lin, G.D. Hutchins, E.G. Chiorean, Pancreatic cancer: utility of dynamic contrast-enhanced MR imaging in assessment of antiangiogenic therapy, Radiology 256 (2) (2010) 441–449, https://doi.org/10.1148/radiol.10091733.
[5] L. Zhong, L. Li, Q.Y. Yao, Preoperative evaluation of pancreaticobiliary tumor using MR multi-imaging techniques, World J. Gastroenterol. 11 (24) (2005) 3756–3761, https://doi.org/10.3748/wjg.v11.i24.3756.
[6] K. Liu, P. Xie, W. Peng, Z. Zhou, Dynamic contrast-enhanced magnetic resonance imaging for pancreatic ductal adenocarcinoma at 3.0-T magnetic resonance: correlation with histopathology, J. Comput. Assist. Tomogr. 39 (1) (2015) 13–18, https://doi.org/10.1097/RCT.0000000000000171.
[7] M.A. Tempero, M.P. Malafa, M. Al-Hawary, H. Asbun, A. Bain, S.W. Behrman, et al., Pancreatic adenocarcinoma, version 2.2017, NCCN clinical practice guidelines in oncology, J. Compr. Canc. Netw. 15 (8) (2017) 1028–1061, https://doi.org/10.6004/jnccn.2017.0131.
[8] E.V. Soloff, A. Zaheer, J. Meier, M. Zins, E.P. Tamm, Staging of pancreatic cancer: resectable, borderline resectable, and unresectable disease, Abdom Radiol (NY). 43 (2) (2018) 301–313, https://doi.org/10.1007/s00261-017-1410-2.
[9] E.A. Eisenhauer, P. Therasse, J. Bogaerts, L.H. Schwartz, D. Sargent, R. Ford, et al., New response evaluation criteria in solid tumours: revised RECIST guideline (version 1.1), Eur. J. Cancer 45 (2) (2009) 228–247, https://doi.org/10.1016/j.ejca.2008.10.026.
[10] Z. Zhang, Z. Wang, R. Zhao, Dynamic contrast-enhanced magnetic resonance imaging of advanced cervical carcinoma: the advantage of perfusion parameters from the peripheral region in predicting the early response to radiotherapy, Int. J. Gynecol. Cancer 28 (7) (2018) 1342–1349, https://doi.org/10.1097/IGC.0000000000001308.
[11] H.H. Li, H. Zhu, L. Yue, Y. Fu, R. Grimm, A. Stemmer, et al., Feasibility of free-breathing dynamic contrast-enhanced MRI of gastric cancer using a golden-angle radial stack-of-stars VIBE sequence: comparison with the conventional contrast-enhanced breath-hold 3D VIBE sequence, Eur. Radiol. 28 (5) (2018) 1891–1899, https://doi.org/10.1007/s00330-017-5193-1.
[12] M. Garcia-Cremades, C. Pitou, P.W. Iversen, I.F. Troconiz, Predicting tumour growth and its impact on survival in gemcitabine-treated patients with advanced pancreatic cancer, Eur. J. Pharm. Sci. 115 (2018) 296–303, https://doi.org/10.1016/j.ejps.2018.01.033.
[13] L. Wu, P. Lv, H. Zhang, C. Fu, X. Yao, C. Wang, et al., Dynamic contrast-enhanced (DCE) MRI assessment of microvascular characteristics in the murine orthotopic pancreatic cancer model, Magn. Reson. Imaging 33 (6) (2015) 737–760, https://doi.org/10.1016/j.mri.2014.08.014.
[14] J.H. Kim, J.M. Lee, J.H. Park, S.C. Kim, I. Joo, J.K. Han, et al., Solid pancreatic lesions: characterization by using timing bolus dynamic contrast-enhanced MR imaging assessment–a preliminary study, Radiology 266 (1) (2013) 185–196, https://doi.org/10.1148/radiol.12120111.
[15] H. Kim, D.E. Morgan, P. Schexnailder, R.M. Navari, G.R. Williams, R.J. Bart, et al., Accurate therapeutic response assessment of pancreatic ductal adenocarcinoma using quantitative dynamic contrast-enhanced magnetic resonance imaging with a point-of-Care perfusion phantom: a pilot study, Invest. Radiol. 54 (1) (2019) 16–22, https://doi.org/10.1097/RLI.0000000000000505.
[16] N.N. Sun, C. Liu, X.L. Ge, J. Wang, Dynamic contrast-enhanced MRI for advanced esophageal cancer response assessment after concurrent chemoradiotherapy, Diagn. Interv. Radiol. 24 (4) (2018) 195–202, https://doi.org/10.5152/dir.2018.17369.
[17] D. Zheng, Q. Yue, W. Ren, M. Liu, X. Zhang, H. Lin, et al., Early responses assessment of neoadjuvant chemotherapy in nasopharyngeal carcinoma by serial dynamic contrast-enhanced MR imaging, Magn. Reson. Imaging 35 (2017) 125–131, https://doi.org/10.1016/j.mri.2016.08.011.
[18] X. Tao, L. Wang, Z. Hui, L. Liu, F. Ye, Y. Song, et al., DCE-MRI Perfusion and Permeability Parameters as predictors of tumor response to CCRT in Patients with locally advanced NSCLC, Sci. Rep. 6 (2016) 35569, https://doi.org/10.1038/srep35569.
[19] M.A. Bali, T. Metens, V. Denolin, M. Delhaye, P. Demetter, J. Closset, et al., Tumoral and nontumoral pancreas: correlation between quantitative dynamic contrast-enhanced MR imaging and histopathologic parameters, Radiology 261 (2) (2011) 456–466, https://doi.org/10.1148/radiol.11103515.
[20] A. Neesse, C.A. Bauer, D. Ohlund, M. Lauth, M. Buchholz, P. Michl, et al., Stromal biology and therapy in pancreatic cancer: ready for clinical translation? Gut (2018), https://doi.org/10.1136/gutjnl-2018-316451.
[21] Y. Binenbaum, S. Na'Ara, Z. Gil, Gemcitabine resistance in pancreatic ductal adenocarcinoma, Drug Resist. Updat. 23 (2015) 55–68, https://doi.org/10.1016/j.drup.2015.10.002.
[22] P.P. Provenzano, C. Cuevas, A.E. Chang, V.K. Goel, D.D. Von Hoff, S.R. Hingorani,

Enzymatic targeting of the stroma ablates physical barriers to treatment of pancreatic ductal adenocarcinoma, Cancer Cell 21 (3) (2012) 418–429, https://doi.org/10.1016/j.ccr.2012.01.007.

[23] L.Y. Ye, Q. Zhang, X.L. Bai, P. Pankaj, Q.D. Hu, T.B. Liang, Hypoxia-inducible factor 1alpha expression and its clinical significance in pancreatic cancer: a meta-analysis, Pancreatology 14 (5) (2014) 391–397, https://doi.org/10.1016/j.pan.2014.06.008.

[24] P. Büchler, H.A. Reber, M. Büchler, S. Shrinkante, M.W. Büchler, H. Friess, G.L. Semenza, O.J. Hines, P. Büchler, H.A. Reber, M. Büchler, et al., Hypoxia-inducible factor 1 regulates vascular endothelial growth factor expression in human pancreatic cancer, Pancreas 26 (1) (2003) 56–64, https://doi.org/10.1097/00006676-200301000-00010.

[25] A. Handra-Luca, C. Lesty, P. Hammel, A. Sauvanet, V. Rebours, A. Martin, et al., Biological and prognostic relevance of mitogen-activated protein kinases in pancreatic adenocarcinoma, Pancreas 41 (3) (2012) 416–421, https://doi.org/10.1097/MPA.0b013e318238379d.

[26] Y. Wang, Z.E. Chen, P. Nikolaidis, R.J. McCarthy, L. Merrick, L.A. Sternick, et al., Diffusion-weighted magnetic resonance imaging of pancreatic adenocarcinomas: association with histopathology and tumor grade, J. Magn. Reson. Imaging 33 (1) (2011) 136–142, https://doi.org/10.1002/jmri.22414.

[27] N. Muraoka, H. Uematsu, H. Kimura, Y. Imamura, Y. Fujiwara, M. Murakami, et al., Apparent diffusion coefficient in pancreatic cancer: characterization and histopathological correlations, J. Magn. Reson. Imaging 27 (6) (2008) 1302–1308, https://doi.org/10.1002/jmri.21340.